Two- to three-dimensional transition during growth and surface alloy formation of Mn on Pd(100)

A. J. Jaworowski,[1] S. M. Gray,[1] M. Evans,[2] R. Ásmundsson,[2] P. Uvdal,[2] and A. Sandell[1]
[1]*Department of Synchrotron Radiation Research, Lund University, Box 118, S-221 00, Lund, Sweden*
[2]*Chemical Physics, Department of Chemistry, Lund University, Box 124, S-221 00 Lund, Sweden*
(Received 17 May 2000; published 5 March 2001; published 5 March 2001)

We show that room temperature growth and alloying of Mn on Pd(100) undergoes a two- to three-dimensional transition. We have correlated the mesoscopic and atomic-scale structures seen in scanning tunneling microscopy to core-level photoemission and Fourier-transform infrared spectroscopy measurements which use CO adsorption as a probe of the surface chemical stoichiometry. In this way we have derived a detailed description of the structure and chemistry of the surface as a function of the Mn coverage. At low coverages, islands of a $c(2\times2)$ Mn-Pd surface alloy grow on unreconstructed 1×1 Pd(100) terraces. An epitaxial $c(2\times2)$ reconstruction which covers the whole surface uniformly is only found for the rather narrow coverage range between approximately 0.7 and 1 ML. Above 1 ML, we observe large, three dimensional Pd-Mn alloy islands situated on a $c(2\times2)$ wetting layer. The top surfaces of these islands have regions of $c(2\times2)$ and (1×1) symmetry, with the (1×1) areas terminated by pure Mn.

DOI: 10.1103/PhysRevB.63.125401 PACS number(s): 68.55.Jk, 68.35.Bs, 78.30.−j

I. INTRODUCTION

Growth and alloying of manganese on various substrates offers the possibility to design materials with interesting magnetic and electronic properties. Pure Mn is known to exist in four phases with different magnetic properties, and epitaxial growth of Mn on suitable substrates has proven to be a fruitful way of stabilizing particular phases.[1–4] Alloying Mn with other metals yielded compounds with interesting magnetoelectronic properties,[2,5–8] and its behavior as a heterogeneous catalyst may also be influenced, since Mn atoms can improve the surface reactivity or the selectivity towards particular surface reactions, e.g., see, Refs. 9–11.

A system that attracted considerable interest over the last few years is Mn deposited on (100) surfaces of late transition metals. One reason for this is that an atomically ordered surface alloy is often formed.

Half a monolayer of Mn deposited above 270 K on Cu(100) and Ni(100) surfaces produces an overlayer with a $c(2\times2)$ structure.[6,12–14] Low-energy electron-diffraction (LEED) intensity curves, Auger electron spectroscopy (AES) and scanning tunneling microscopy (STM) measurements suggest that the topmost layer is an alloy in which equal amounts of Mn and substrate atoms form a checkerboard pattern. Calculations indicate that the surface alloy is magnetically stabilized.[6] Furthermore, on Ni(100) and Cu(100) surfaces, it is possible to prepare several other ordered epitaxial alloys of varying thicknesses depending on the Mn coverage and temperature.[12,13] However, annealing of thick Mn films (4–6 ML) to 500–600 K again results in a $c(2\times2)$ structure, which is assumed to be epitaxial.

Deposition of 0.5-ML Mn on Ag(100) also yields a $c(2\times2)$ LEED pattern, but, interestingly, this system is found to be unstable at room temperature (RT): after deposition, the $c(2\times2)$ islands are progressively replaced by two-dimensional (2D) Ag(1×1) islands.[15] However, increasing the Mn content stabilizes the $c(2\times2)$ structure considerably.

Growth of Mn on Pd(100) is particularly interesting because of the small misfit between the spacing of the square surface lattice of Pd(100) ($a=2.75$ Å) and the cubic lattice parameter of pure δ-Mn at RT as obtained from band-structure calculations ($a_0=2.78$ Å).[16] The Pd_3Mn bulk alloy was the subject of a number of investigations, including studies of its magnetic properties and the solubility of hydrogen in the alloy matrix.[17,18] This alloy has a structure in which layers similar to pure Pd(100) alternate with Pd-Mn checkerboard layers. Pd-Mn is also of general interest because of its catalytic activity: for example, the reduction of CO by NO occurs to a much greater extent on Pd-Mn particles supported on SiO_2 than on clean Pd.[19,20] The reason for this is probably an enhanced likelihood of NO dissociation caused by the presence of surface Mn.

Two previous papers dealing with the growth of Mn on Pd(100) used LEED intensity analysis to derive structural information.[2,8] During the initial stages of room-temperature growth, a weak $c(2\times2)$ LEED pattern was observed between estimated Mn coverages of 1.5–6 ML, with the best pattern at about 2 ML. Brief anneals of these films to about 570 K improved the LEED pattern significantly. Based on the LEED spectra it was proposed that the as-deposited surface consists of a strongly buckled Pd-Mn surface layer with a Mn sublayer above a Pd sublayer, with this relation becoming reversed upon annealing. Calculations of LEED intensities based on the bulk Pd_3Mn structure produced a moderate fit to the data from the annealed surface. The termination of the surface alloy was suggested to be a flat checkerboard layer. Depositions of larger amounts of Mn above 6 ML resulted in a 1×1 LEED pattern, but annealing produced a weak $c(2\times2)$ pattern, and Auger electron spectroscopy showed that considerable Pd enrichment of the surface had occurred.

There are also a few recent studies of the adsorption properties of the Pd(100)-Mn-$c(2\times2)$ surface alloy. The adsorption of CO and C_2H_4 on a clean and O-precovered alloy

surface was investigated using high-resolution electron-energy-loss spectroscopy (HREELS).[21,22] Also, in a very recent paper, we presented an extensive photoelectron spectroscopy (PES) study of the adsorption of small molecules (CO, CO_2, NO, and O_2) on the Pd(100)-Mn-$c(2\times2)$ surface, including fundamental adsorption properties, coadsorption, and surface reactions.[23] There are also theoretical studies of the adsorption of CO and NO on the (100) surface of the Pd_3Mn alloy.[24,25]

It has become apparent that in the characterization of the Pd-Mn bimetallic system, the most important task is to determine the Mn growth mechanism and the structure of the resulting surface and interface. In this paper, we address the fundamental growth and alloying behavior of Mn on Pd(100) using STM, core level PES, and Fourier transform infrared (FTIR) spectroscopy. We find clear evidence for a 2D-3D transition during the growth of the surface alloy, i.e., the growth is initially two dimensional but becomes three dimensional at a certain coverage. This is in stark contrast to the pure 2D alloy growth suggested for Mn on Ni(100), Cu(100), and Ag(100).[12,13,15] We also present information about how the atomic structure of the surface varies as a function of Mn coverage, and show that it is possible to prepare surfaces with various compositions. A flat $c(2\times2)$ alloy covering the whole surface is found only for a rather narrow coverage range of approximately 0.7–1 ML. Above 1 ML, we observe large 3D alloy islands situated on a $c(2\times2)$ wetting layer, clearly demonstrating that mesoscopic effects must be considered in the initial stages of alloy growth.

II. EXPERIMENTAL DETAILS

The core-level photoemission data were recorded at beamline I311 and beamline 22 (BL22) at the Swedish national synchrotron light facility, MAX-lab. I311 is a new undulator-based beamline for studies in the vacuum ultraviolet and with soft x rays, while BL22 is bending magnet beamline optimized for measurements in the soft-x-ray region.[26] The endstations at both beamlines have two separate chambers for measurements and sample preparation. A large hemispherical electron energy analyzer of the Scienta type is used to record the photoelectron spectra. The total-energy resolution for C 1*s* spectra, measured at a photon energy of 400 eV, is 140–280 meV at I311 and 500 meV at BL22. Mn 2*p* spectra were measured at $h\nu=750$ eV. All spectra were obtained at normal emission, and all binding-energy values are relative to the Fermi edge.

The STM data were obtained with a commercial UHV microscope.[27] Sample cleaning and Mn deposition was carried out in one chamber, and surface characterization by AES, LEED, and STM was performed in a separate chamber in which the base pressure is always below 5×10^{-11} mBar. STM tips were made from electrochemically etched tungsten wire, cleaned in vacuum by Ar^+ sputtering and radiative heating. The condition of the tip was monitored by imaging Si(111) and Si(001) samples. The images presented here are unprocessed, except that a best-fit plane has been subtracted from the data.

The FTIR experiments were performed in an UHV chamber (base pressure 7×10^{-11} torr) connected to a N_2 purged Bruker Vector 22 Fourier-transform infrared spectrometer. The spectra were recorded with 2-cm^{-1} resolution below 100 K. The background was recorded after a 600-K flash. The chamber was also equipped with a cylindrical mirror analyzer for Auger electron spectroscopy, and a bare quadrupole mass-spectrometer for temperature-programmed desorption measurements.

The Pd crystal was cleaned by sputtering with 2.5-kV Ar+ ions at 900 K, followed by a 1-min anneal at 1150 K. In addition, several oxygen treatments were used to remove residual carbon. During these, the oxygen pressure was kept at 2×10^{-8} mBar while the temperature was cycled between 400 and 900 K. After oxygen treatments the crystal was flashed to 1100 K. Surface cleanliness was checked by PES, AES, and/or STM depending on the experimental system used.

Mn was evaporated using a metal flake (Goodfellow, purity 99.98+%) placed inside a resistively heated tungsten coil. The sample was always held at RT during deposition. Coverage calibration of Mn was first carried out with a quartz microbalance in order to obtain photoemission and Auger reference spectra. The evaporation rate (typically 0.1–0.2 ML/min) could then the accurately monitored by the Mn 2*p* PES intensity or by the Mn/Pd Auger ratio. During evaporation the pressure was kept below 1×10^{-9} mBar. The Mn coverage is given in terms of monolayers, where 1 ML equals the number of Pd atoms in one atomic layer of Pd(100). In order to form the well-ordered $c(2\times2)$ alloy, the as-deposited surface was annealed to 570 K for 3 min, following a scheme given previously.[21,22]

III. RESULTS

A. Establishing the growth mode

Figure 1 shows STM pictures for coverages of 0.3 ± 0.1 and 0.7 ± 0.1 ML of Mn on Pd(100) both before and after annealing to 570 K. At 0.3 ML the LEED pattern is a fuzzy $c(2\times2)$ which improves after annealing. The STM images show that at this coverage Mn creates 2D islands on the Pd(100) terraces. Annealing results in a more well-ordered surface containing fewer, larger islands, and on which steps and island edges more closely follow the high-symmetry directions of the surface. The apparent height of the steps and islands varies from 1.8 to 2.3 Å, which should be compared to the constant step height of 2.0 Å found for clean Pd(100), and the value of 1.95 Å expected from the known structure of the Pd lattice. The dominant step orientation is along ⟨001⟩-type directions, although some steps and islands edges also follow ⟨011⟩ directions. The diagonal rows of Mn atoms in the proposed $c(2\times2)$ surface alloy are also parallel to ⟨011⟩ directions, which suggests that some areas of ordered alloy are present at this Mn coverage, as is confirmed by the adsorption behavior of CO (see below). The variation in step height can therefore be explained as being due to variations in the local structures on the upper and lower terraces. A detailed atomic-resolution STM investigation of this surface observed this local structure, and will be presented

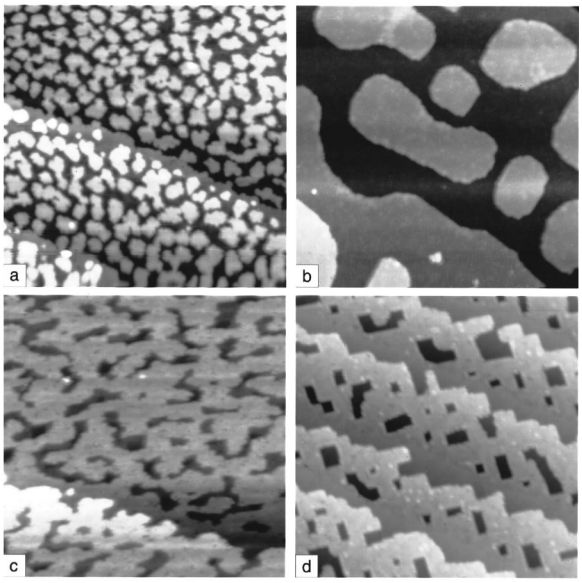

FIG. 1. STM constant-current topographs of annealed and unannealed Mn-Pd(100) surfaces taken at Mn coverages of 0.3 ± 0.1 and 0.7 ± 0.1 ML. (a) 0.3 ML of Mn, unannealed (image width $=600$ Å, Vsample 0.1 V, Itip$=0.1$ nA). (b) 0.3 ML of Mn annealed to 570 K (600 Å, -1.0 V, 0.01 nA). (c) 0.7 ML of Mn, unannealed (400 Å, 1.0 V, 0.01 nA). (d) 0.7 ML of Mn annealed to 570 K (600 Å, 0.005 V, 1.0 nA).

elsewhere;[28] however, it is worth noting here that on all these surfaces atomic resolution was only obtained with STM after annealing, despite the fact that LEED showed a $c(2\times2)$ LEED pattern on the as-deposited surface. This suggests that when the STM reveals atomic detail it is imaging a surface state which can only be observed when there is a higher degree of surface order than the minimum needed to create a LEED pattern.

At 0.7 ML the islands coalesce, and upon annealing form well-ordered flat terraces with rectangular monolayer pits. At this coverage LEED shows a clear $c(2\times2)$ pattern after Mn deposition, which further improves upon annealing. The apparent height of both the steps and the monolayer pit edges is 2.0 ± 0.1 Å, and the orientation of both sorts of structure is now almost exclusively along $\langle011\rangle$ directions. The uniformity of the surface structures, the appearance of a single step height that matches the monolayer spacing of bulk Pd, and the fact that monolayer pits are often seen to merge with steps on the downhill side of a terrace but never on the uphill side all indicate that at this coverage the surface consists of a single reconstruction.

Doubling the Mn content has a dramatic effect on the surface topography. Figure 2 shows STM topographs for a coverage of 1.5 ± 0.1 ML before and after annealing. The unannealed 1.5-ML Mn surface is filled with large islands, several atomic layers high, which run over and across (2.0 ± 0.1)-Å-high steps that separate otherwise flat terraces. Upon annealing these islands grow and coalesce, in the process becoming less dendritic and better oriented along $\langle001\rangle$ and $\langle011\rangle$ directions.

Determining the surface structure from the STM images is made difficult by the fact that the STM cannot directly identify chemical species. Also, our atomic-scale images from these surfaces always contain ''jumps'' caused by atomic-scale changes in the tip structure. However, such jumps cannot alter the surface's observed periodicity and orientation, so we can determine the local symmetry of the surface, even if the detailed atomic arrangements are unclear from the STM data alone. Figure 3 shows atomic-scale images from the wetting layer surrounding the islands and from the flat top on one of the large islands. The wetting layer has a uniform $c(2\times2)$ symmetry, interrupted only by steps and point defects. Patches of $c(2\times2)$ symmetry are also observed on top of the islands, but they are intermixed with areas of 1×1 symmetry. All these spacings and orientations were calibrated against low-drift images of the clean 1×1 Pd(100) surface, as well as test samples of Si(111) and Si(100).

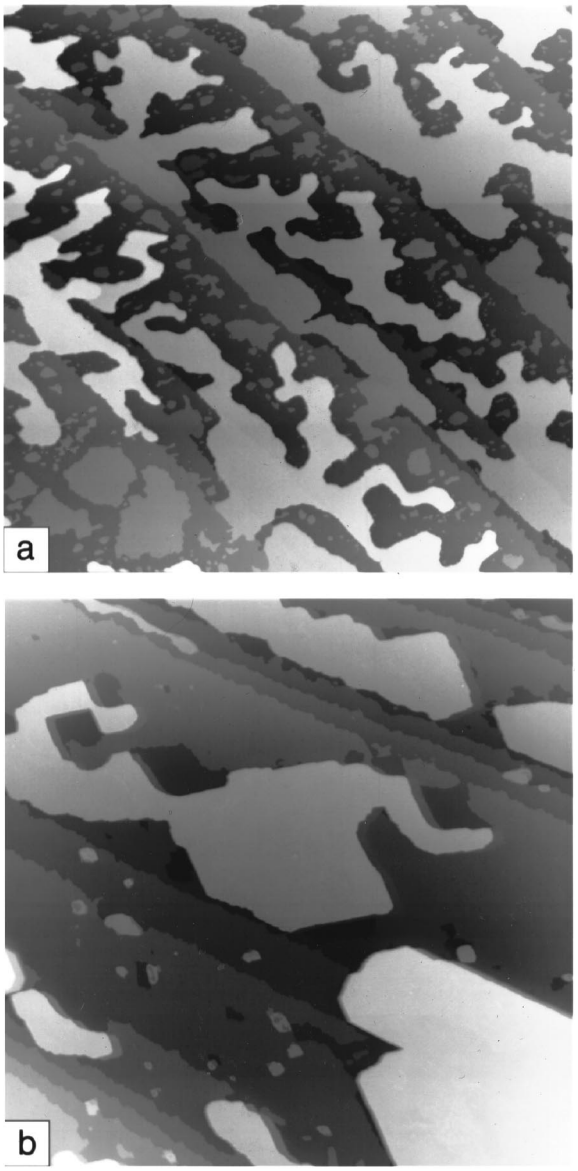

FIG. 2. STM topographs for 1.5 ± 0.1 ML of Mn on Pd(100). (a) As deposited at room temperature (4000 Å, 1.5 V, 0.01 nA). (b) After annealing to 570 K (4000 Å, -3.0 V, 0.01 nA).

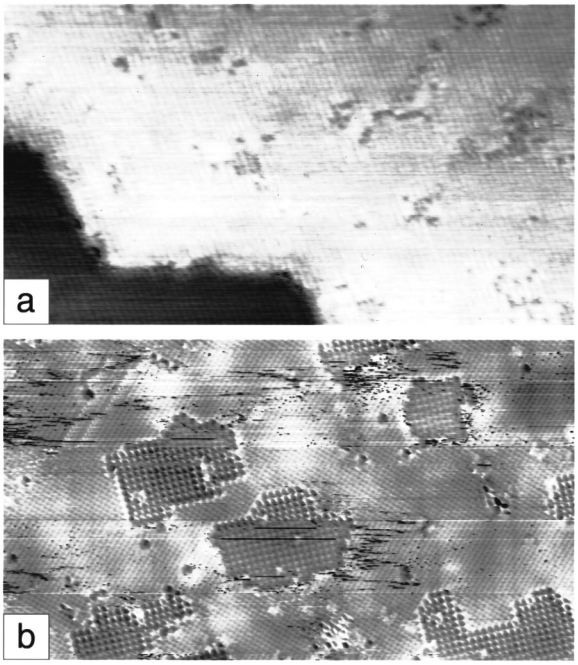

FIG. 3. Atomic resolution STM images of the annealed 1.5-ML Mn surface shown in Fig. 2(b). (a) The $c(2\times2)$ wetting layer (300 Å, 0.005 V, 3.0 nA). (b) On top of one of the large islands, where patches of $c(2\times2)$ and (1×1) symmetry coexist ($X\times300$ Å, 0.005 V, 3.0 nA).

Before annealing, the islands cover about 50% of the total surface area, but afterward this figure decreases to around 30%. On the other hand, the average height of the islands increases with annealing, such that their apparent volume remains approximately constant. If we assume that the islands are pure, bulk Mn, this volume corresponds to 2.0 ±0.1 ML of Mn atoms. However, the $c(2\times2)$ symmetry observed on the wetting layer indicates that it must contain some of the deposited Mn. If we assume that the wetting layer has the proposed checkerboard pattern, the fact that it occupies 70% of the post-annealing surface indicates that at least 0.35 ML of Mn must be bound up in the wetting layer. Since we only deposited 1.5 ML of Mn, the islands can contain at most 1.15 ML, and it is therefore almost certain that the islands are composed of an alloy of Mn and Pd. A highly improbable expansion of the Mn lattice must otherwise be supposed to explain the observed discrepancy.

The changeover from a flat surface with only single-layer steps to 3D island growth is characteristic of the Stranski-Krastanov growth mode, and for simplicity's sake we will refer to the growth as Stranski-Krastanov growth here. However, it is important to emphasize that the traditional thermodynamic picture, driven by the surface and interface energies of the substrate and overlayer, may be complicated here by a contribution from the free energy associated with alloy formation.

The Stranski-Krastanov transition is also apparent in the plot of the integrated intensity of the Mn $2p_{3/2}$ photoemission peak as a function of Mn deposition time (not shown). The Mn $2p$ intensity follows a reasonably straight line up to around or just below 1 ML. At this point, the signal suddenly levels off before it starts to increase slowly in a somewhat complicated manner. The AES uptake curve shows very similar behavior, and both are consistent with the Stranski-Krastanov growth mode.

The complicated growth behavior justifies a brief comment about coverage calibrations. In the first LEED and EELS studies,[2,8] AES data interpreted in terms of a layer-by-layer growth were used to determine the Mn coverage. The best $c(2\times2)$ LEED pattern was thus reported to occur at a coverage of 2 ML. In our own first PES study of this system,[23] we measured a Mn $2p$ growth curve, and interpreted the kink as due to completion of the first Mn layer. The ''$c(2\times2)$'' alloy was then prepared using twice the deposition time, in accordance with the previously published results.[2,8,21,22] However, our present STM/LEED results show that the 0.7-ML coverage gives the best epitaxial $c(2\times2)$ surface prior to annealing, and a very well-defined uniform $c(2\times2)$ surface after annealing. The $c(2\times2)$ pattern at higher coverages is produced from an inhomogeneous surface containing large 3D islands. We have recalibrated our old data, and found that the coverages do lie between 1.5 and 2.0 ML, i.e., in the 3D island growth regime. We conclude that the earlier LEED/EELS studies are either based on erroneous coverage calibrations or, like our own study, have measured data for alloy surfaces containing 3D Stranski-Krastanov islands.

To summarize, STM, LEED, and AES data show that Mn grows on Pd(100) according to the so-called Stranski-Krastanov mode. Initially, the overlayer grows layer by layer, but at a coverage around 1 ML the overlayer collapses into 3D alloy islands surrounded by a $c(2\times2)$ wetting layer.

B. Adsorption of CO

1. CO on heated surfaces

Additional information about the surface composition at different Mn coverages can be obtained by using the adsorption of CO as a probe of the surface chemical stoichiometry. We start by discussing the more well-ordered surfaces which are obtained after annealing. Figure 4 shows C 1*s* core-level photoelectron spectra for CO adsorbed on four different surfaces: clean Pd(100), and three different Mn coverages of 0.4, 0.7, and 1.5 ML. In all four cases, the CO dosage was 10–20 L, and the sample temperature was at 100–120 K during the gas admission.

In the C 1*s* PE spectrum for CO/Pd(100) we observe one sharp peak at a binding energy (BE) of 285.9 eV (labeled ''1''), in agreement with previous results. This peak is associated with CO in bridge sites, which is the only site occupied on Pd(100).[29–31]

Next we turn to the highest Mn coverage, 1.5 ML, which, if we take into account the coverage calibration issues discussed above, corresponds to the substrate surface studied in our previous PES paper,[23] and can be explained using the results presented there. The C 1*s* spectrum is complicated: with two peaks at BE's of 286.5 and 285.4 eV (labeled ''2'' and ''3,'' respectively). There is also an intense tail on the high BE side. By comparison with other systems, in particular CO/1-ML Pd/Mo(110), we were able to identify peak 2

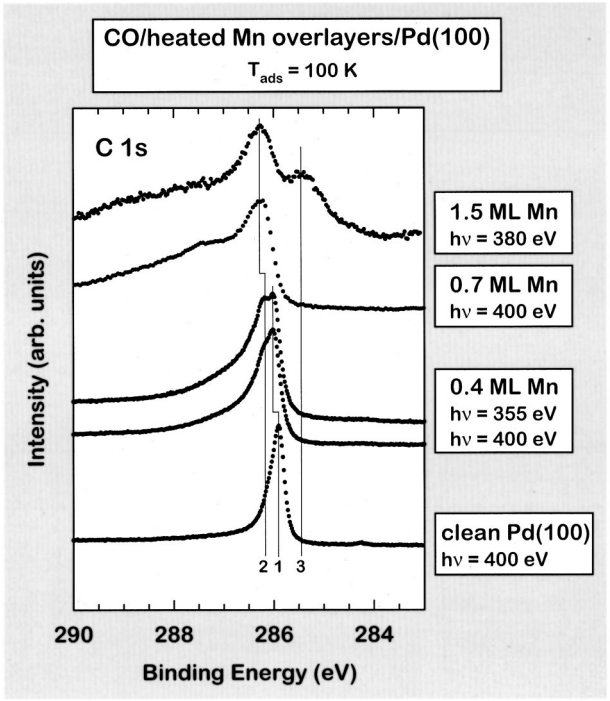

FIG. 4. C 1*s* photoelectron spectra for CO adsorbed on clean Pd(100) and Pd(100) with increasing Mn coverage: 0.4, 0.7, and 1.5 ML. The Mn-modified surfaces were prepared by deposition at RT followed by heating to 570 K for 3 min. Peak 1 is CO adsorbed on Pd in bridge sites, peak 2 is the main peak for CO adsorbed on Pd in on-top geometry, and peak 3 is due to CO adsorbed on Mn (see the text for a full discussion).

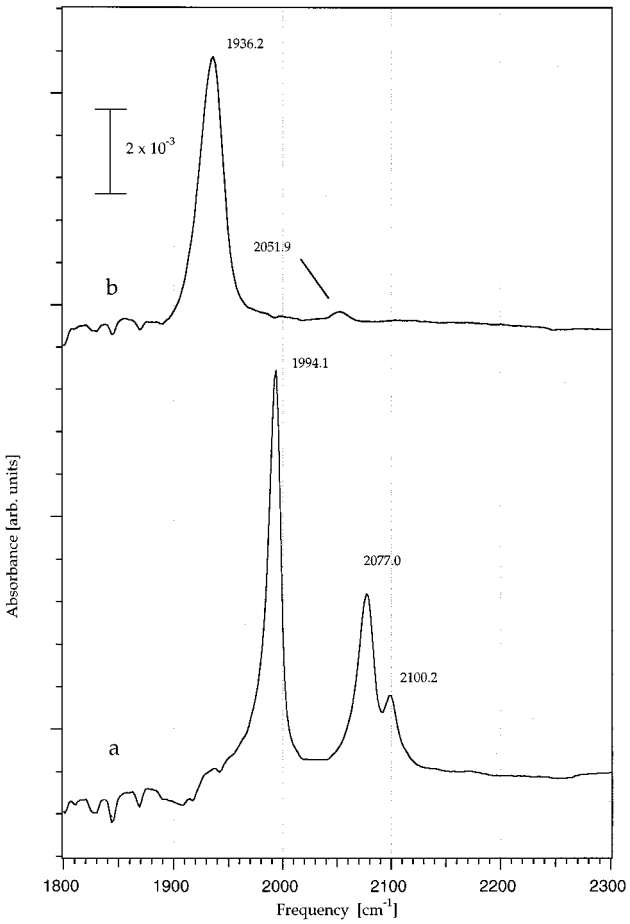

FIG. 5. (a) FT-IR spectra of 20-L CO adsorbed (<100 K) on Pd(100), covered with 0.25-ML Mn preheated to 570 K. (b) After annealing to 390 K.

and the high BE tail as being due to upright CO molecules adsorbed on top of Pd atoms. The high BE tail consists of so-called shake-up features, an effect which is most apparent for weakly bonded CO species. Note that the desorption temperature for CO on top of Pd lies around 250 K, which places it in the same category as, for example, CO/Cu(100), a system in which prominent shake-ups are also seen.[32] We confirmed that this CO species is indeed coordinated to Pd by the observation of a related component in the Pd 3*d* PES spectrum.

Peak 3 is due to a second CO species, which can be isolated on the surface since it remains bound up to temperatures of approximately 400 K. However, in contrast to the more weakly bonded species, these CO molecules did not give rise to a shifted Pd 3*d* component. Furthermore, the C 1*s* BE is significantly lower than the BE found for CO adsorbed on Pd(100). We therefore concluded that this species is instead coordinated to Mn atoms.

With this information in mind, we may now consider the coverage 0.7 ML. This is the interesting situation where our STM images showed that the surface is completely covered by an epitaxial $c(2\times2)$ alloy [see Fig. 1(d)]. The C 1*s* spectrum displays a peak at 286.5 eV and additional features at higher BE's which, again, is characteristic for CO adsorbed on top of Pd. If we compare this spectrum to the 1.5-ML spectrum and the C 1*s* spectrum for CO/1-ML Pd/Mo(110) where only on-top CO is found,[32] it can be concluded that CO on top of Pd is the only species present. Annealing the CO overlayer to RT results in desorption of all the molecules, which further corroborates this assignment. Consequently, on the pure $c(2\times2)$ Pd-Mn alloy surface, CO only occupies the Pd atoms and coordinates in an on-top fashion. This observation is in agreement with theoretical predictions by Delbecq and Sautet.[24]

Finally, the C 1*s* spectrum for a coverage of 0.4 ML displays a doublet structure with one feature at 286.0 eV (''1'') and another at 286.2 eV (''2''). Changing the photon energy from 400 to 355 eV changes the intensity ratio between these features. This is typical behavior when two different CO species occupying different sites are present on the surface. In such a case, changing the kinetic energy of the photoelectron gives rise to intensity variations caused by diffraction effects. These variations are sensitive to the local surrounding of the molecule, and can be used as a fingerprint of the adsorption site.[33] The presence of intensity variations here excludes the possibility that peak 2 is a satellite to peak 1, since the intensity ratio between a main peak and a satellite does not change with the photoelectrons' kinetic energy. Because of the close proximity in BE to the peak found for CO on the clean Pd(100) surface, we assign the low BE feature, peak 1, to CO in bridge sites, and for similar reasons identify peak 2 as due to CO adsorbed on top of Pd.

We have also investigated the adsorption of CO on the annealed Mn/Pd(100) surfaces using FT-IR spectroscopy. Figure 5 shows the results for CO on a 0.25-ML Mn/Pd(100) surface which had been annealed at 570 K prior to CO adsorption. This surface corresponds to the STM image shown in Fig. 1(b) above. The surface was exposed to 20-L CO at a surface temperature below 100 K [Fig. 5(a)]. Subsequently, the sample was heated to 390 K, [Fig. 5(b)].

The adsorption of CO on the clean Pd(100) (Refs. 30 and 34) and hydrogen covered Pd(100)$p(1\times1)$H (Ref. 35) surfaces was previously studied in detail using IR, EELS, and LEED. It was demonstrated that on the clean Pd(100) surface only bridge sites are occupied,[29] in agreement with the PES data described above. The C-O stretch frequency increases continuously from ~1900 to ~2000 cm^{-1} as the CO coverage is increased from 0.1 to 0.8 ML.[34] It was also shown that at low temperature (20 K) CO only occupies on-top sites on the Pd(100)$p(1\times1)$H surface.[35] The CO stretch mode frequency for this on-top site was 2105 cm^{-1} (261 meV).

The adsorption of CO on the Mn/Pd(100) surface at low temperature results in three different CO species with CO stretch frequencies at 1994, 2077, and 2098 cm^{-1}, as is clearly shown in Fig. 5(a). It follows from the PES data above that all three CO species are coordinated to Pd. The mode at 1994 cm^{-1} is a signature of CO adsorbed in bridge sites on the clean Pd(100) surface. The frequency is consistent with a local CO coverage of approximately 0.8 ML, consistent with the high CO dose of 20 L. The appearance of two additional CO species at 2077 and 2098 cm^{-1} on the Mn/Pd(100) surface are obviously related to the Mn-induced modification of the surface. Both frequencies are consistent with CO in on-top sites on metal surfaces, which typically are observed in the 2065–2105 cm^{-1} region.[30,32,35]

Figure 5(b) shows that on heating to 390 K the CO species associated with Mn-induced surface modification desorb, and the CO concentration on the Mn-free Pd(100) surface is reduced. The remaining CO species observed at 1936 cm^{-1} is assigned to CO adsorbed in bridge sites on the clean Pd(100) surface. The frequency is consistent with a local CO coverage of approximately 0.4 ML. The weak feature at 2052 cm^{-1} is attributed to readsorption of small amounts of CO on to the Mn modified surface.

To summarize, PES and FTIR data of CO adsorbed on the annealed Mn/Pd(100) surfaces show that CO only adsorbs on top of Pd on the epitaxial $c(2\times2)$ alloy, in contrast to clean Pd(100) where CO adsorbs in bridge sites. That two CO species (on-top and bridge) can be identified in the PES and FTIR data for small coverages of Mn (0.25 and 0.4 ML) shows that clean Pd(100) surface areas and Mn-modified $c(2\times2)$ areas coexist, that is, the $c(2\times2)$ alloy initially grows as 2D islands and the Mn atoms are not uniformly dispersed over the surface. Finally, the surfaces containing 3D islands have Mn sites to which CO molecules can bond, even at temperatures high enough to desorb them from both pure Pd and from Pd incorporated into a $c(2\times2)$-Mn reconstruction.

2. CO on unheated surfaces

We can now consider CO adsorption onto the less well-ordered surfaces obtained by room-temperature deposition of Mn with no subsequent anneal. Figure 6 shows C 1*s* spectra for CO adsorbed onto Pd(100) surfaces with Mn coverages of 0.7 and 1.2 ML. At 0.7 ML we find two peaks at 286.3 and 285.3 eV (1 and 2, respectively), with the former having a substantial high BE tail. The spectrum shows a strong resemblance to the C 1*s* spectrum for CO on the post-anneal 1.5-ML Mn surface shown in Fig. 4, and the assignment of peak 1 as due to CO on top of Pd and peak 2 as due to CO on Mn is therefore straightforward. Heating the surface to 500 K only leads to CO desorption; no dissociation was found, as is as evident from the absence of a peak at 282–283 eV.

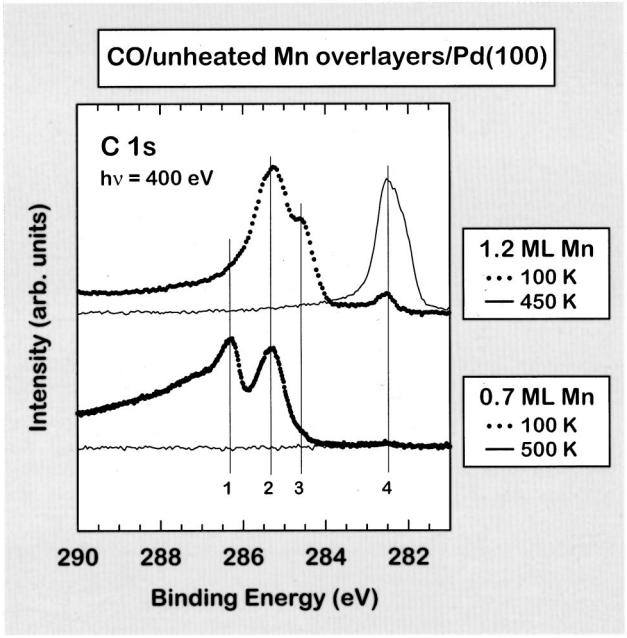

FIG. 6. C 1*s* spectra for CO adsorbed on Pd(100) onto which Mn has been deposited at RT without subsequent annealing. Peak 1 is due to molecular CO adsorbed on top of Pd atoms. Peaks 2 and 3 are due to molecular CO adsorbed on Mn. Peak 4 is associated with atomic carbon, and indicates that some CO has dissociated.

The top spectra show the corresponding data for 1.2-ML Mn. This situation behaves very differently: After CO adsorption at 100 K, a peak is found at 285.3 eV (2), with a low BE shoulder (3). Based on the above findings, we can assign peak 2 as due to CO on Mn. Heating to 450 K effectively dissociates CO as inferred by the appearance of a strong peak at 282.5 eV (4).

Comparing the results in Fig. 6 to those obtained on surfaces annealed before gas adsorption, it can be concluded that the all the as-deposited surfaces contain Mn atoms onto which CO may adsorb. For the lower coverage surfaces these Mn atoms lose their ability to bond to CO when the surface is annealed. When 3D islands are present the surface retains Mn atoms capable of bonding to CO even after annealing, but the ability to dissociate CO found for the as-deposited surface is effectively quenched.

IV. DISCUSSION

From the STM results it is clear that the growth of Mn on Pd(100) must be reassessed in the light of the discovery that

a Stranski-Krastanov 2D-3D transition occurs during growth of the overlayer. However, although the STM can reveal the overall surface morphology and the atomic-scale symmetry of the first layer, by itself it cannot investigate such matters as the surface's chemical stoichiometry. By combining STM observations with our PES and FT-IR measurements, we can follow the development of the surface during Mn deposition on both the mesoscopic and the atomic scale.

At coverages below 0.7-ML Mn deposition followed by annealing to 570 K yields well-defined $c(2\times2)$ islands separated by 1×1 regions of clean Pd(100). This surface composition might perhaps be the most interesting with respect to catalytic properties, since the $c(2\times2)$ patches interact strongly with O_2 and NO,[23,36] whereas the 1×1 areas are likely to maintain the excellent (CO) oxidation properties of Pd(100).[37] In particular, CO oxidation reactions at RT might be worth studying, since at this temperature it is possible to have spatially separated ''reaction centers'' due to the fact that no CO adsorbs on the $c(2\times2)$ areas whereas both NO and O_2 dissociate on these areas.[23,36]

An important finding is that the coverage regime where one obtains a complete epitaxial $c(2\times2)$ surface layer is rather narrow. Below 0.7-ML areas of pure 1×1 Pd appear, and above about 1-ML 3D alloy islands form. A $c(2\times2)$LEED pattern can be observed over a wide range of coverages, but neither this, nor the sharp kink in the AES or PES Mn uptake curves, should be taken to indicate layer-by-layer growth, and in the absence of STM measurements great care must be taken to ensure that the surface is genuinely homogeneous. Conversely, within this coverage range the surface does exhibit a high degree of uniformity, and the epitaxial $c(2\times2)$ reconstruction appears promising as a substrate for further studies using area-averaging surface science techniques.

Before the epitaxial $c(2\times2)$ surface is annealed, CO adsorbs on both Mn and Pd, but after annealing only CO adsorbed on top of Pd can be observed. The loss of the CO adsorption capability of the Mn atoms is in line with the previous study,[8] which suggested that the Mn atoms go beneath the surface Pd layer upon heating. However, because of the coverage calibration issues raised by our observation of Stranski-Krastanov growth, it is not clear whether this investigation was undertaken in the 2D or 3D growth region. Our results are compatible with the idea that Mn atoms move to subsurface sites upon annealing, but could also be interpreted as meaning that Mn loses its ability to bind to CO when part of a fully ordered $c(2\times2)$ Pd-Mn surface alloy, and that it is disorder in the as-deposited surface that allows CO to adsorb on to Mn atoms.

In the 3D growth regime, the volume estimate using STM shows that the islands must consist of a mixture of Pd and Mn. This is strongly corroborated by the adsorption of CO on as-deposited 1.2-ML Mn. At this coverage we expect that 3D islands have started to form, but in PES only CO on Mn is observed, showing that the surface layer is mostly comprised of Mn atoms. There is simply not enough Mn to cover the surface and simultaneously to form 3D islands of the observed size, and we deduce that the interior of the islands must be formed of a Pd-Mn alloy. Furthermore, a clear majority of the CO molecules dissociate upon heating, which is in stark contrast to the behavior of CO on the as-deposited epitaxial $c(2\times2)$ alloy. As an early transition metal, pure Mn is expected to be very active toward CO dissociation.[38] We therefore conclude that a large part of this surface consists only of Mn atoms and that, on surfaces showing 3D growth, both the islands and their surrounding wetting layers have Mn-rich surfaces before annealing.

Our results show that a Pd enrichment of the surface occurs upon annealing of the 1.5-ML coverage, but that the annealed surface still contains a substantial amount of Mn atoms onto which CO can adsorb. Again, this is in contrast to the epitaxial $c(2\times2)$ alloy, where no CO adsorption is observed after annealing. This raises the question of what sort of Mn atoms the CO are bonding to. The STM pictures show that after annealing the 3D islands are terminated by a mixture of $c(2\times2)$ and 1×1 domains, while the wetting layer is entirely of $c(2\times2)$ symmetry. The most obvious atomic-scale difference between the epitaxial $c(2\times2)$ layer formed at 0.7 ML and the 3D islands found at 1.5 ML is the appearance of 1×1 domains on the tops of the islands, and it is reasonable to supposed that these consist of pure Mn. However, the PES results on the unheated 1.2-ML surface indicate that CO adsorbed on 1×1 Mn is likely to dissociate upon heating, but out of four preparations of an annealed 1.5-ML Mn surface covered with CO, we observed dissociation upon heating only once.

This inconsistency is best explained by variations in the composition of the islands' surface layer. Our STM results indicate that the relative areas occupied by the 1×1 and $c(2\times2)$ reconstructions vary from island to island, and is at least partially related to the island's thickness. The size and distribution of Stranski-Krastanov islands would be expected to change with annealing temperature and time, as well as with Mn coverage, and the step density of the underlying Pd(100). STM measurements appear to confirm that this is the case. It therefore seems reasonable that at coverages where 3D island growth occurs the exact surface topology, and in particular the amount of Mn available for CO adsorption, can vary quite widely. A more elaborate investigation of how the surface structure varies with annealing time and temperature is needed in order to clarify this behavior.

V. CONCLUSIONS

Using STM, PES and FT-IR measurements, we have investigated the structure of as-deposited and annealed Mn overlayers on Pd(100). At low coverages, below 0.7 ML, room-temperature deposition leads to the formation of $c(2\times2)$ islands separated by 1×1 regions of pure Pd. Between 0.7 and 1 ML, a flat $c(2\times2)$ alloy covers the whole surface. Annealing these surfaces to 570 K results in a better-ordered surface, as indicated by an improvement in the $c(2\times2)$LEED pattern and the appearance of atomic-scale detail in STM topographs. In addition, the as-deposited surface contains Mn atoms onto which CO can adsorb, but after annealing CO only bonds to Pd, adopting an on-top geometry in areas with $c(2\times2)$ symmetry and occupying

bridge sites on clean 1×1 Pd(100). This suggests that Mn goes subsurface when annealed, but it is also possible that Mn loses its ability to bond to CO when it is incorporated into the fully ordered $c(2\times2)$ Pd-Mn surface alloy.

When the Mn coverage exceeds about 1 ML, large 3D islands start to form. The overall growth mode is therefore of a Stranski-Krastanov type, implying that the Mn/Pd(100) system behaves differently from Mn/Ni(100) and Mn/Cu(100). Two important consequences of this are, first, that future surface science investigations which use area-averaging techniques must carefully calibrate the Mn coverage; and second, that RT growth of Mn films on Pd(100) is expected to produce very rough interfaces.

Above the transition to 3D island growth, deposition yields islands and a wetting layer which are both mostly terminated by Mn. The 3D islands must contain a significant amount of Pd, since their volume is too large for them to be made of pure bulk Mn. Subsequent annealing to about 570 K ripens the islands so that they become larger and less dendritic. After annealing, the wetting layer shows a $c(2\times2)$ symmetry in STM topographs, and a general morphology that is very similar to the $c(2\times2)$ expitaxial layer. The top surfaces of the islands have regions of $c(2\times2)$ and (1×1) symmetry, and CO adsorption implies that the 1×1 areas consist of pure Mn.

ACKNOWLEDGMENTS

We thank the staff at MAX-lab for their invaluable experimental assistance. This work was financially supported by the Swedish Natural Science Research Council (NFR). S.M.G. thanks the Craaford foundation and the Wallenberg foundation for financial support.

[1] P. Eckerlin and H. Kandler, in *Structure Data of Elements and Intermetallic Phases*, edited by K.-H. Hellwege, Landolt-Börnstein, New Series, Group III, Vol. 6 (Springer-Verlag, New York, 1971).
[2] D. Tian, S. C. Wu, F. Jona, and P. M. Marcus, Solid State Commun. **70**, 199 (1989).
[3] B. T. Jonker, J. J. Krebs, and G. A. Prinz, Phys. Rev. B **39**, 1399 (1989); Y. U. Idzerda, B. T. Jonker, W. T. Elam, and G. A. Prinz, J. Appl. Phys. **67**, 5385 (1990).
[4] W. F. Egelhoff, Jr., I. Jacob, J. M. Rudd, J. F. Cochran, and B. Heinrich, J. Vac. Sci. Technol. A **8**, 1582 (1990).
[5] P. Schieffer, M.-H. Tuilier, M.-C. Hanf, C. Krembel, G. Gewinner, D. Chandesris, and H. Magnan, Phys. Rev. B **57**, 15 507 (1998).
[6] M. Wuttig, Y. Gauthier, and S. Blügel, Phys. Rev. Lett. **70**, 3619 (1993).
[7] S. Blügel, Appl. Phys. A: Mater. Sci. Process. **63**, 595 (1996), and references therein.
[8] D. Tian, R. F. Lin, F. Jona, and P. M. Marcus, Solid State Commun. **74**, 1017 (1990).
[9] Y. J. Mergler, A. van Aast, J. van Delft, and B. E. Nieuwenhuis, J. Catal. **161**, 310 (1996).
[10] A. B. Hayden, P. Pervan, and D. P. Woodruff, J. Phys.: Condens. Matter **7**, 1139 (1995).
[11] H. Lu, E. Janin, M. E. Davila, C. M. Pradier, and M. Göthelid, Surf. Sci. **408**, 326 (1998).
[12] M. Wuttig, T. Flores, and C. C. Knight, Phys. Rev. B **48**, 12 082 (1993).
[13] R. G. P. van der Kraan and H. van Kempen, Surf. Sci. **338**, 19 (1995).
[14] O. Rader, W. Gudat, C. Carbone, E. Vescovo, S. Blügel, R. Kläsges, W. Eberhardt, M. Wuttig, J. Redinger, and F. J. Himpsel, Phys. Rev. B **55**, 5404 (1997).
[15] P. Schieffer, C. Krembel, M. C. Hanf, and G. Gewinner, Phys. Rev. B **55**, 13 884 (1997).
[16] V. L. Moruzzi, P. M. Marcus, and P. C. Pattnaik, Phys. Rev. B **37**, 8003 (1988).
[17] P. Önnerud and Y. Andersson, Solid State Commun. **101**, 433 (1997).
[18] D. Rodric, P.-J. Ahlzén, and Y. Andersson, Solid State Commun. **78**, 767 (1991).
[19] J. F. Trillat, J. Massardier, B. Moraweck, H. Praliaud, and A. J. Renouprez (unpublished).
[20] A. El Hamdaoui, G. Bergeret, J. Massardier, M. Primet, and A. J. Renouprez, J. Catal. **148**, 47 (1994).
[21] S.-C. Wu, J.-F. Jia, K. Wu, S.-H. Lu, R.-G. Zhao, and D.-Z. Wang, Surf. Sci. **312**, 167 (1994).
[22] J.-F. Jia, K. Wu, S.-H. Lu, R.-G. Zhao, X.-M. Wei, S.-C. Wu, and D.-Z. Wang, Surf. Sci. **338**, 69 (1994).
[23] A. Sandell, A. J. Jaworowski, A. Beutler, and M. Wiklund, Surf. Sci. **421**, 116 (1999).
[24] F. Delbecq and P. Sautet, Phys. Rev. B **59**, 5142 (1999).
[25] F. Delbecq and P. Sautet, Surf. Sci. **442**, 338 (1999).
[26] J. N. Andersen, O. Björnholm, A. Sandell, R. Nyholm, J. Forsell, L. Thånell, A. Nilsson, and N. Mårtensson, Synchrotron Radiat. News **4**, 15 (1991). Also see http://www.maxlab.lu.se/beamline/hd-bl.htm.
[27] Omicron Vakuumphysik GMbH, Tanusstein, Germany.
[28] A. J. Jaworowski, S. Gray, M. Evans, R. Ásmundsson, P. Uvdal, and A. Sandell (unpublished).
[29] J. P. Biberian and M. A. van Hove, Surf. Sci. **118**, 443 (1982).
[30] P. Uvdal, P.-A. Karlsson, C. Nyberg, S. Andersson, and N. V. Richardson, Surf. Sci. **202**, 167 (1988).
[31] J. N. Andersen, M. Qvarford, R. Nyholm, S. L. Sorensen, and C. Wigren, Phys. Rev. Lett. **67**, 2822 (1991).
[32] A. Sandell, A. Beutler, R. Nyholm, J. N. Andersen, S. Andersson, P. A. Bruhwiler, N. Mårtensson, J. Libuda, K. Wolter, O. Seiferth, M. Bäumer, H. Kuhlenbeck, and H.-J. Freund, Phys. Rev. B **57**, 13 199 (1998).
[33] See for example: A. Beutler, E. Lundgren, R. Nyholm, J. N. Andersen, B. J. Setlik, and D. Heskett, Surf. Sci. **396**, 117 (1998).
[34] A. Ortega, F. M. Hoffman, and A. M. Bradshaw, Surf. Sci. **119**, 79 (1982).
[35] C. Nyberg and L. Westerlund, Chem. Phys. Lett. **185**, 445 (1991).

[36] A. J. Jaworowski, S. Gray, R. Ásmundsson, P. Uvdal, and A. Sandell (unpublished).
[37] T. Engel and G. Ertl, in *The Chemical Physics of Solid Surfaces and Heterogeneous Catalysis*, edited by D. A. King and D. P. Woodruff (Elsevier, Amsterdam, 1982), Vol. 4.
[38] J. C. Campouzano, in *The Chemical Physics of Solid Surfaces and Heterogeneous Catalysis*, edited by D. A. King and D. P. Woodruff (Elsevier, Amsterdam, 1990), Vol. 3A.